

# A MEMS SINGLET OXYGEN GENERATOR

Tyrone F. Hill, Luis F. Velásquez-García, Benjamin A. Wilhite<sup>†</sup>, Klavs F. Jensen, Alan H. Epstein, and Carol Livermore<sup>1</sup>

Massachusetts Institute of Technology, Cambridge, MA 02139 USA

<sup>†</sup>Department of Chemical Engineering, University of Connecticut, Storrs, CT 06269 USA

## ABSTRACT

Abstract— The design, creation, and demonstration of a singlet oxygen generator (SOG) that operates on the microscale are presented. The micro singlet oxygen generator ( $\mu$ SOG) chip creates singlet delta oxygen ( $O_2(^1\Delta)$ ) in an array of packed bed reaction channels fed by inlets with pressure drop channels to equalize flow. An integrated capillary array separates the liquid and gas byproducts, and microscale cooling channels remove excess heat of reaction. The fabrication process and package are designed to minimize collisional and wall deactivation of  $O_2(^1\Delta)$ . Flow behavior and capillary separation are characterized over a range of plenum (gas outlet) pressures and feed rates. The testing setup enables measurement of  $O_2(^1\Delta)$  via optical emission measurements and mass spectrometry. Spontaneous decay of the  $O_2(^1\Delta)$  molecule into its triplet state is observed, confirming the production of  $O_2(^1\Delta)$ .

*Index Terms*— singlet oxygen, Chemical Oxygen Iodine Laser (COIL), MEMS

## INTRODUCTION

Singlet delta oxygen,  $O_2(^1\Delta)$  or spin-excited molecular oxygen, is valuable as a reactant for organic synthesis and as an energy carrier for the Chemical Oxygen-Iodine Laser (COIL). COIL is attractive for applications requiring very high average powers, light weight, and overall system compactness. COIL provides a promising alternative to  $CO_2$  lasers for industrial machining. A lower emission wavelength (1.315 $\mu$ m vs. 10.6  $\mu$ m for  $CO_2$ ) results in more efficient coupling to metals, reducing the power needed for welding and cutting. The lower wavelength also results in smaller spot size, so COIL systems offer higher machining resolution, and enables fiber-optic beam delivery for greater flexibility. In a flowing gas laser such as COIL, the waste heat flows out with the reactant exhaust gas stream so the laser average power is not limited by cooling, as are most high energy solid state lasers. The COIL system is scalable to average power output in excess of 1 MW.

COIL systems are chemical lasers in which iodine acts as the lasing species [1]. Population inversion of the gain medium is sustained by collisions between ground state iodine atoms ( $I(^2P_{3/2})$ ) and  $O_2(^1\Delta)$ .  $O_2(^1\Delta)$  is a metastable molecule which may be synthesized through the highly exothermic multiphase chemical

reaction of gaseous  $Cl_2$  with an aqueous mixture of concentrated  $H_2O_2$  and KOH, commonly referred to as basic hydrogen peroxide (BHP). The laser application of  $O_2(^1\Delta)$  generation requires a high yield to sustain laser emission, where yield is defined as the fraction of product oxygen in the  $O_2(^1\Delta)$  state. High conversion of  $Cl_2$  to  $O_2(^1\Delta)$  is achieved by effective mixing of the gas and liquid reagents. Once produced, singlet-oxygen may deactivate into ground-state oxygen by gas-phase collisions with water vapor, other oxygen or helium diluent molecules, and by heterogeneous collisions with either solid- or fluid surfaces. Thus, the reactor design must provide large surface areas for initial  $O_2(^1\Delta)$  generation, balanced by subsequent rapid separation of gas and liquid phases, while maintaining low pressures (~50-250 torr) to minimize homogeneous deactivation and low temperatures (< 0°C) to minimize water vaporization and subsequent deactivation. The present work shows that the challenges of high yield, thermal management, and product separation can be successfully addressed by a MEMS-based approach to  $O_2(^1\Delta)$  generation.

Before continuing the discussion of  $\mu$ SOG development, it is useful to define the excitation states of molecular oxygen discussed. An oxygen molecule has four electrons in its outer p-subshell. The  $O_2(^3\Sigma)$  state (“triplet” or ground state oxygen) has three electrons in one spin state and the fourth in the other, while the  $O_2(^1\Delta)$  state has two electrons in each of the ‘spin up’ and ‘spin down’ configurations [2]. The near resonance between  $O_2(^1\Delta)$  state and the  $I(^2P_{1/2})$  state of atomic iodine makes  $O_2(^1\Delta)$  an ideal pumping source for laser emission.

Generation of  $O_2(^1\Delta)$  for COIL was first demonstrated by McDermott et al. in 1978[1].  $Cl_2$  gas was bubbled through an aqueous solution of 90% wt  $H_2O_2$  and 6M NaOH in a sparger at a flow rate of 6000 sccm, producing singlet delta oxygen. After passing through a cold trap to remove moisture and unreacted chlorine, the product gas was injected into a mixture of  $I_2$  and Ar. The yield obtained was approximately 40%. The system was cooled by a combination of dry ice and ethanol. McDermott’s method was successful, but it is limited by significant deactivation of  $O_2(^1\Delta)$  gas before separation from the liquid phase. Subsequent SOG configurations have employed either jets of BHP droplets mixed with  $Cl_2$  [3] or rotary SOG configurations [4]. In rotary SOGs a film of BHP on the surface of a rotating wheel is exposed to a  $Cl_2$  stream, resulting in  $O_2(^1\Delta)$  production at the interface. However, these configurations have their limitations: a small gas – liquid contact area for rotary SOGs, and a large volume for the jet configuration. The present work demonstrates that arrays of

<sup>1</sup> Sponsored by Defense Advanced Research Projects Agency, Tactical Technology Office (TTO); Micro Chemical Oxygen-Iodine Laser (COIL) Program; ARPA Order No. T171/00, Program Code: 4G10; Issued by DARPA/CMO under Contract No. MDA972-04-C-0140.

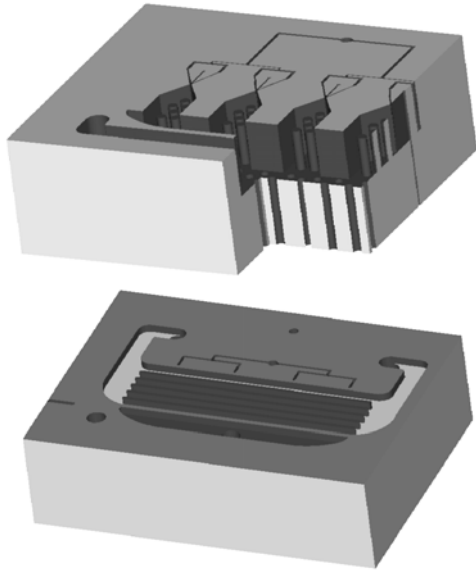


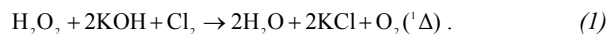
**Figure 1.** (Top) A simplified 3D cutaway of the SOG device, showing bifurcated inlets, pressure drop channels, reaction channels, and capillary separator array. (Bottom) The lower wafer contains gas bifurcations, cooling channels, and inlet/outlet ports.

MEMS-based SOGs can address the shortcomings of these previous designs, thus providing greater  $O_2(^1\Delta)$  flow per unit volume.

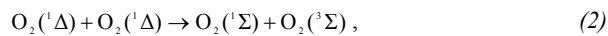
This paper first presents a conceptual discussion of SOG operation and details of the device design. The packaging scheme and testing rig are then summarized. Flow functionality of the chip was demonstrated for a variety of gas and liquid feed rates. Experimental results that confirm the production of singlet delta oxygen are presented, and comparisons with macro-scale SOGs are made.

## SOG CONCEPT

SOGs typically produce  $O_2(^1\Delta)$  by mixing gaseous chlorine and BHP, according to the chemical equation



Often the  $Cl_2$  is mixed with a buffer gas (He or  $N_2$ ) in order to raise the total pressure of the stream. After generation,  $O_2(^1\Delta)$  may be deactivated by several mechanisms, the most prominent being collisions between  $O_2(^1\Delta)$  molecules,



and wall interactions



Because reactants are distributed between two different phases, maximizing the contact area between gas and liquid phases is critical to obtain high yields. Previous studies have shown that microreactors offer advantages with respect to mass and thermal transfer characteristics [5]. The  $\mu$ SOG maximizes contact area

between phases by conducting the reaction in an array of packed bed reaction channels. Pressure-drop channels located upstream of each packed bed aid in equalizing gas and liquid flow throughout the microdevice.

A previous analytical study evaluated the feasibility of microscale  $O_2(^1\Delta)$  generation [6]. Using standard MATLAB numerical simulation techniques and estimates of physical parameters, key SOG dimensions and operating points were optimized. The optimum device dimensions (with respect to the estimated parameters) included a reaction channel length of 0.516 cm, 0.25 cm long pressure drop channels, a 1 cm section for gas and liquid flow distribution, and an optimal He: $Cl_2$  flow rate of 175 sccm. The dimensions employed in the present  $\mu$ SOG mask design were largely based on the results and conclusions of this study.

## DEVICE DESIGN AND FABRICATION

The  $\mu$ SOG consists of a two-wafer silicon stack capped by a Pyrex layer. The upper silicon layer contains symmetrically bifurcated BHP inlets and pressure drop channels to distribute the reactants evenly across the chip, an array of 32 reaction channels to enable the multiphase reaction of BHP and  $Cl_2$ , and a capillary separator array to remove spent BHP and waste products. The pressure drop channels have a width of 25  $\mu\text{m}$  and a depth of approximately 20  $\mu\text{m}$ . The reaction channels are each 6.1 mm long, 630  $\mu\text{m}$  wide, and 300  $\mu\text{m}$  high. They contain posts of diameter 70  $\mu\text{m}$  and pitch 90  $\mu\text{m}$ , which increase the contact area between gas and liquid phases. This post-bed configuration is a two-dimensional approximation of a conventional packed-bed, providing reduced pressure drops while alleviating the need for subsequent packing of reaction channels. The separator contains approximately 10,000 20  $\mu\text{m}$  holes which remove the liquid effluent via capillary forces [7].

The lower silicon layer contains cooling channels to remove heat generated during the reaction, enabling low-temperature operation, along with supporting structures: inlets, outlets, and bifurcated gas distribution. The 19 cooling channels are of width 300  $\mu\text{m}$  and height 300  $\mu\text{m}$ . The BHP and  $Cl_2$  inlets are 1 mm in diameter; all other inlet and outlet connections are 2 mm in diameter. Finally, the chip contains a thermocouple port for *in situ* temperature monitoring. The die size was set at 3.6 cm x 2.8 cm to accommodate packaging. The features on both layers were created using a deep reactive ion etch (DRIE) process.

Starting materials for the SOG were two 625  $\mu\text{m}$  thick <100> DSP silicon wafers purchased from Silicon Quest (San Jose, CA) and one 625  $\mu\text{m}$  thick Pyrex wafer obtained from Bullen Ultrasonics of Eaton, OH. First, a 0.5  $\mu\text{m}$  silicon dioxide protection layer was grown on each wafer by thermal oxidation. A nested mask was used to create 20  $\mu\text{m}$  deep pressure drop channels, 350  $\mu\text{m}$  high posts, and the separator bed on the reaction chamber wafer. Next, a wet oxidation step was used to grow a 0.5  $\mu\text{m}$  protective oxide layer over the posts. This layer prevented erosion of the posts during subsequent long DRIE steps. The capillary holes were formed by lithographically patterning the wafer backside and DRIE. Finally, all remaining thin films were removed from both sides.

The first step in creating the lower wafer was the deposition of a 4  $\mu\text{m}$  PECVD oxide hard mask on both surfaces. Photoresist was spun onto both sides of the wafer, and cooling channel and inlet/outlet patterns were patterned in the films on the top and bottom surfaces, respectively. DRIE was used to form the cooling

TABLE I  
EXPERIMENTAL CONDITIONS

Parameter	Value
He Flowrate	37 sccm
Cl <sub>2</sub> Flowrate	13 sccm
BHP Flowrate	1 ml/min
BHP Delivery Pressure	40 psig
Plenum Pressure	100 torr
Separator Pressure	20 torr
Chip Temperature	3 C
BHP Supply Temperature	-10 C

channels and liquid waste collection area on the top surface. Finally, flow inlets and outlets were etched in the backside by DRIE. Selected fabrication cross sections for both wafers are given in Fig. 2.

After removing the remaining films from the cooling wafer, the stack was fusion bonded. Following bonding, the stack was annealed in N<sub>2</sub>, and 0.4 μm PECVD Si-rich nitride was deposited on it. The nitride forms a protective layer over the reaction wafer surface as well as the sidewalls of the capillary separator features and inlets, preventing the BHP from attacking the silicon during operation. Finally, the Pyrex wafer was anodically bonded to the stack and the chips diced.

## PACKAGING

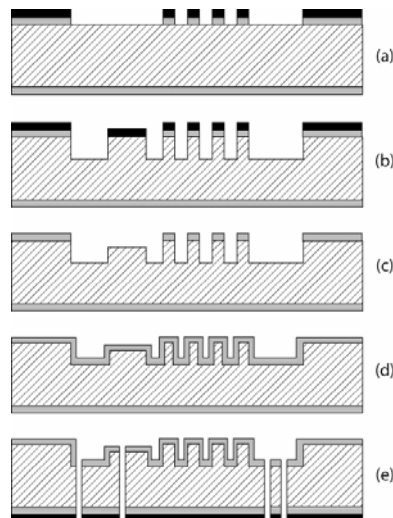
The finished chips were packaged using teflon tubing and fiberglass-reinforced epoxy. Teflon connections were chosen to give the setup flexibility and to minimize alignment issues. Stainless steel Swagelok ferrules were used to hold the tubing in place prior to gluing. The BHP inlet was connected to 1/16" tubing. All other connections were made with 1/8" teflon with the exception of the gas outlet, which was connected directly to a quartz optical cell for O<sub>2</sub>(<sup>1</sup>Δ) detection.

A significant issue when selecting packaging materials was minimizing deactivation of O<sub>2</sub>(<sup>1</sup>Δ). Glass surfaces are particularly attractive for the gas outlet, owing to a wall deactivation coefficient that is half that for the best metals and an order of magnitude lower than teflon [8].

## EXPERIMENTAL SETUP

Because of the toxic and corrosive nature of chlorine gas and hydrogen peroxide, all experiments are performed inside a ventilated cabinet. As shown schematically in Figure 4, mass flow controllers regulate both helium and chlorine supply to the μSOG. A second helium flow is employed to pump BHP from a thermostated reservoir to the μSOG. The helium pressure (and thus the BHP flow rate) is regulated by a pressure controller. After flowing through the chip and separator, the BHP is collected in a second thermostated reservoir. Both reservoirs were maintained at temperatures of -10°C - 20°C to minimize BHP decomposition. Ensuring that the BHP is properly cooled is critical for safety; at temperatures above 50°C, H<sub>2</sub>O<sub>2</sub> decomposition is accelerated and the solution can be explosive. Before reaching the vacuum pump, both lines pass through liquid nitrogen cooling traps in order to condense water vapor and unreacted chlorine. The gas outlet is also connected to a mass spectrometer through a 189 μm diameter

## Reaction Wafer



## Cooling Wafer

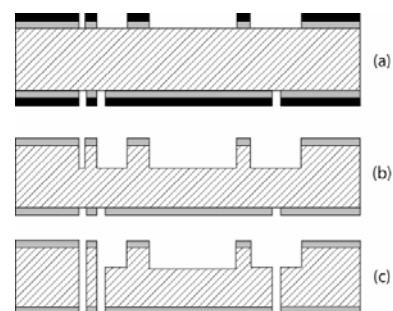


**Figure 2.** μSOG fabrication process: (gray denotes SiO<sub>2</sub>, black denotes resist) Reaction wafer— (a) reaction channels are patterned in SiO<sub>2</sub> and resist layers, (b) & (c) nested mask process creates pressure drop and reaction channels, (d) SiO<sub>2</sub> protection layer grown over features, (e) separator holes and inlets are pattern and etched from the backside. Cooling wafer— (a) front and backside features patterned with resist and SiO<sub>2</sub>, (b) & (c) a silicon dioxide layer is used as a hard mask to etch features on both surfaces.

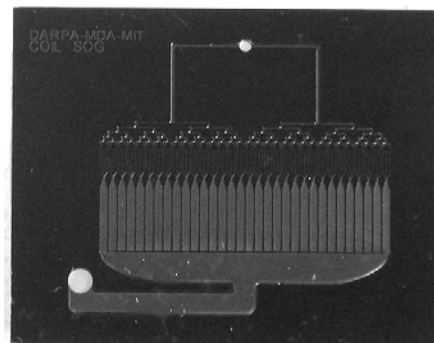


**Figure 3.** Photograph of a completed chip

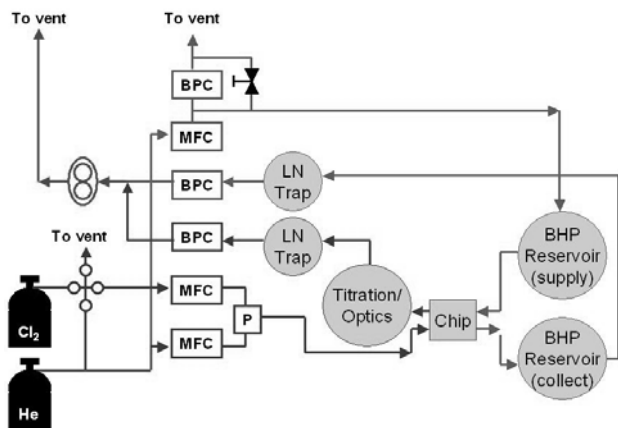


Figure 4. Schematic of experimental apparatus

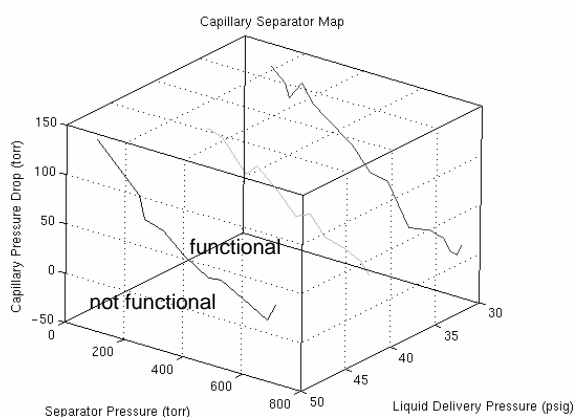


Figure 5. Map of capillary separator performance

glass capillary line, allowing sampling of a portion of the plenum stream. The entire setup is served by an external chiller (Julabo, Allentown, PA), which circulated a silicone-based cooling fluid through the chip and both the BHP supply and collection reservoirs.

Prior to operation with Cl<sub>2</sub> and BHP reagents, the  $\mu$ SOG flow functionality was investigated using inert He and distilled (DI) water. The two functionalities of primary importance are (i) gas-liquid hydrodynamics in the packed-bed reaction channels, and (ii) extent of liquid removal by the capillary separator. Both are critical to device performance, as the former directly effects the rate of O<sub>2</sub>(<sup>1</sup>Δ) generation, and the latter impacts O<sub>2</sub>(<sup>1</sup>Δ) yield.

Two unique modes of gas-liquid flow were observed in the present device. At low to moderate gas and liquid flows, a steady flow pattern is observed, in which the liquid flows continuously as a wetted film along both the channel walls and partially wets the posts, while the gas flows through the remaining voids. Once developed, gas-liquid interfaces remained stationary with the majority of reactor volume being gas, resulting in limited interaction of the two phases. At high gas and liquid flow rates, the gas-liquid interface begins to fluctuate rapidly, resulting in an unsteady liquid flow which may enhance gas-liquid mixing. The former, steady flow, was observed under all reacting conditions investigated.

The capillary separator performance was also investigated using

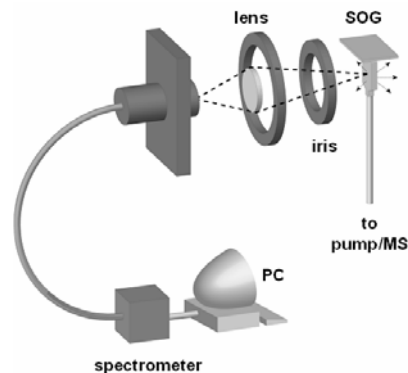


Figure 6. Illustration of emission measurement concept

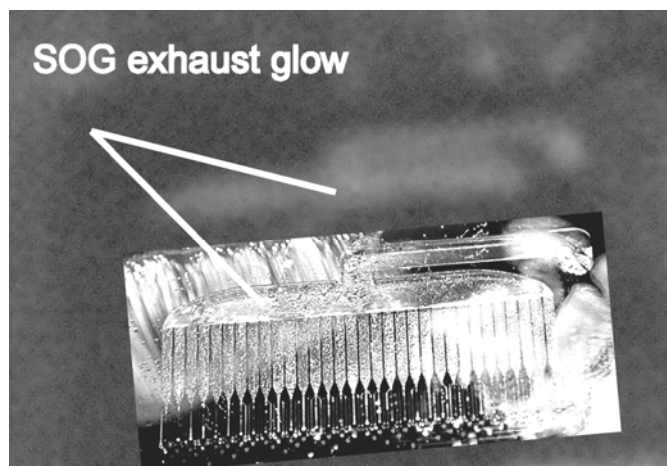
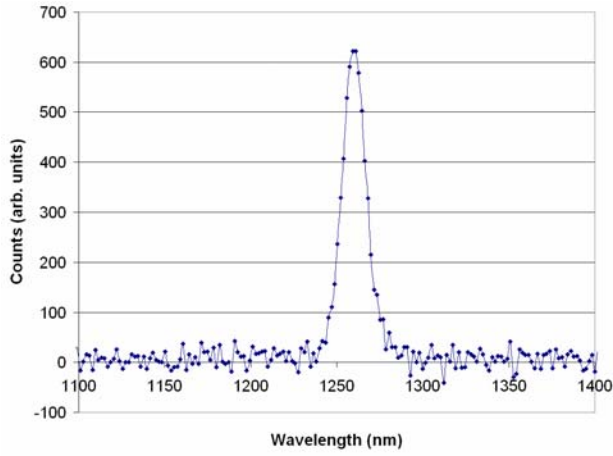


Figure 7. (Background) pink glow from O<sub>2</sub>(<sup>1</sup>Δ) dimer emission. (Foreground) Superimposed image of  $\mu$ SOG.

He and H<sub>2</sub>O. The separator operates on the basis of liquid capillary pressure; during operation the 20  $\mu$ m holes are filled with liquid, which is driven through the holes and out of the chip by an imposed pressure drop. The capillary pressure of the liquid film resists flow of gas through these same holes, thus effectively separating the two phases. It was observed (shown in Figure 5) that as the liquid flow increases, the necessary capillary pressure drop likewise increases. As separator pressure decreases, the required pressure drop across the separator also increases.

Although it is relatively straightforward to confirm O<sub>2</sub>(<sup>1</sup>Δ) generation, quantitatively measuring the yield is a significant challenge. Typically SOG performance is determined in the context of a complete COIL system; heuristics are used to estimate yield from output power along with various losses and efficiencies in the system [9]. Out of the array of methods of measuring and quantifying yield [4,10,11], one of the simpler options was chosen. Production was confirmed by observing the O<sub>2</sub>(<sup>1</sup>Δ) dimer emission, which appears as a pink glow. The number of O<sub>2</sub>(<sup>1</sup>Δ) molecules in a given volume can be calculated by measuring the spontaneous emission produced by the O<sub>2</sub>(<sup>1</sup>Δ) - O<sub>2</sub>(<sup>3</sup>Σ) transition at a wavelength of 1268 nm. The chlorine utilization, or percentage of chlorine converted to oxygen, can be determined via mass spectrometry. These two measurements were used together to calculate O<sub>2</sub>(<sup>1</sup>Δ) yield.

The emission measurement was done on a 4 cm x 1 cm quartz



**Figure 8.** IR Spectra from  $\mu$ SOG showing peak from  $O_2(^1\Delta) - O_2(^3\Sigma)$  transition

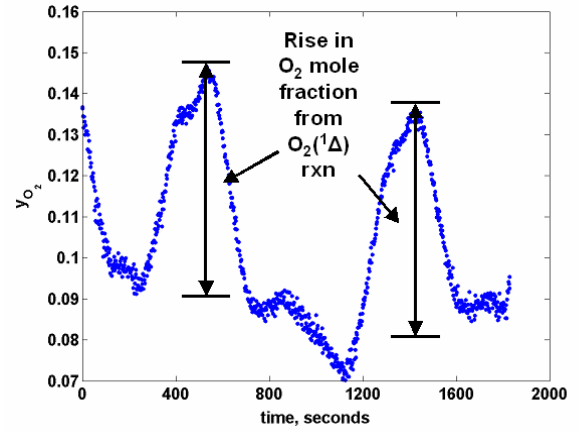


**Figure 9.** Mass spectrometer signal showing oxygen mole fraction as a function of time during the experimental run

CONSTANTS FOR EQUATIONS 4-8

Symbol	Quantity	Units
$I$	LED current ( used in calibration)	Amperes
$V$	LED voltage (used in calibration)	Volts
$\eta_{LED}$	LED efficiency	dimensionless
$X$	Fraction of illumination captured by optics (calibration)	dimensionless
$\gamma$	Spectrometer efficiency correction factor	dimensionless
$\Delta t$	Integration time	seconds
$\theta_{\text{samp}}$	Solid angle sampled by optics (experiment)	steradians
$y_x$	Mole fraction of species x	dimensions
$P_{\text{oxygen}}$	Partial pressure of oxygen	torr
$V_{\text{optics}}$	Column of cuvette sampled by optics	$\text{cm}^3$
$C_m$	Measured counts	Arbitrary units
$\tau$	Singlet oxygen lifetime	seconds

cuvette (Starna, Atascadero, CA), which was connected directly to the  $\mu$ SOG gas outlet. An Ocean Optics (Dunedin, FL) NIR512 InGaAs array spectrometer was used to analyze photons from the spontaneous emission. Light was relayed from the cuvette to the spectrometer by focusing optics. A lens ( $f\#$  1.9) was placed 13.1 cm from the cuvette and 8.1 cm from the spectrometer's fiber input. The emission setup, described in Figure 8, was calibrated using an infrared LED. Sample gas for the mass spectrometer was collected through a glass capillary connected to the plenum line. The signal was calibrated using an 80%:20% He: $O_2$  tank, with other conditions matching those of the experimental run.

TABLE II  
COMPARISONS WITH OTHER SOGS

SOG type	$O_2(^1\Delta)$ FLOW RATE PER UNIT VOLUME ( $\times 10^{-4}$ MOL/S/L)
Sparger	2.3
Jet-type	23
Disk-type	87
$\mu$ SOG (this work)	90

## TESTING

Prior to testing, the BHP solution is prepared within the supply reservoir as follows. First 20 ml of a 50 wt% aqueous  $H_2O_2$  solution (Aldrich) is chilled to  $20^\circ\text{C}$  in the jacketed reservoir. Then, 20 ml of a 50 wt% aqueous KOH solution is slowly added, such that the mixture temperature never exceeds  $10^\circ\text{C}$ . Significant heat is released upon mixing of KOH and  $H_2O_2$ , and thus care must be taken to avoid overheating of the BHP solution. When complete, the BHP reservoir is sealed and pressurized with He to initiate BHP flow through the  $\mu$ SOG. He flow is then initiated through the chip, and the separator and plenum pressures are slowly lowered to 100 and 80 torr respectively. When the pressures are stable and the separator is working properly, the chlorine flow is introduced in pulses of several minutes duration each. Table 1 summarizes the test conditions. A visible pink glow from the dimer emission, shown in Figure 7, is observed in the chip's capillary separator. The emission measurement was made 2.5 cm below the SOG gas outlet. Spectra from the  $O_2(^1\Delta) - O_2(^3\Sigma)$  transition are shown in Figure 8. The oxygen mole fraction of the output stream, given in Figure 9, shows an increase in  $O_2$  content with the  $Cl_2$  pulses.

## DISCUSSION

In order to determine  $O_2(^1\Delta)$  yield, concentrations of both  $O_2(^1\Delta)$  and total oxygen must be calculated for the volume interrogated by the optics. The calibration factor  $\beta$ , defined as

$$\beta = \frac{I * V * \eta_{LED} * X * \gamma * \Delta t}{\text{counts}} \quad (4)$$

relates energy from the  $O_2(^1\Delta) - O_2(^3\Sigma)$  transition to spectrometer counts. Because the calibration and experiment involve two different wavelengths (940 and 1268 nm respectively), the correction factor  $\gamma$  is needed to account for variations in spectrometer sensitivity. The efficiency of the calibration LED,  $\eta_{LED}$ , was calculated as approximately 15% using the half angle of emission and assuming a Gaussian intensity profile. The number of  $O_2(^1\Delta)$  photons collected by the optics is

$$N_{SD} = \frac{C_m * \beta * 4\pi * \tau}{h\nu * \Delta t_{exp} * \theta_{samp}} \quad (5)$$

The isotropic nature of the  $O_2(^1\Delta)$  emission is reflected by the solid angle correction factor ( $4\pi/\theta_{samp}$ ). The oxygen mole fraction of the output stream was calculated from the mass spectrometry data and shows an increase in  $O_2$  content as a function of the  $Cl_2$  pulses

$$r_{Cl} = \frac{\Delta y_{O_2}}{y_{Cl}} \quad (6)$$

Considering the rise in  $O_2$  mole fraction and the original  $Cl_2$  mole fraction of 25%,  $r_{Cl}$  was determined to be 24%. After using  $r_{Cl}$  to determine  $P_{oxygen}$ , the total number of  $O_2$  molecules is calculated as

$$N_{tot} = \frac{P_{oxygen} V_{optics}}{RT} \quad (7)$$

The yield,

$$Y = \frac{N_{SD}}{N_{tot}} \quad (8)$$

at the measurement point is between 77-100%. The uncertainty in the yield measurement is primarily due to 4% error in the distance of the focusing optics from the cuvette. This uncertainty is reflected in both the calculation of  $V_{optics}$  and in the final yield number.

The analytical model described in [6] predicts a yield of 86% at the gas outlet for these flow conditions and for a chlorine utilization of 24%, which is consistent with the experimental data obtained. The high yield of the  $\mu$ SOG makes it competitive with the existing COIL technologies [3, 4, 12]. Table 2 offers a comparison between the performance of the  $\mu$ SOG and published macroscale SOGs. The  $O_2(^1\Delta)$  molar flow rate per unit reaction volume is  $90 \times 10^{-4}$  mol/l/s, which is comparable to the most efficient  $O_2(^1\Delta)$  flow rates reported for macro-scale SOGs.

These results were obtained for flow rates near the minimums of the parameter space (gas and liquid flowrates) explored in the previous theoretical study [6]. Results from that study predict higher yields at increased throughputs, owing to higher chlorine conversions. Further improvements in performance are possible via improved gas-liquid mixing at higher flows. Present results were obtained under steady-flow patterns in which gas and liquid contact area comprised a small portion of the available reaction channel surface. As a result, chlorine utilization was significantly lower than expected theoretically, and therefore less  $O_2(^1\Delta)$  was created. At increased gas and liquid flows, unsteady-flow patterns develop, resulting in improved gas-liquid interaction.

## CONCLUSIONS

We have demonstrated the first production of  $O_2(^1\Delta)$  in a microscale device for COIL applications. The yield was determined through a combination of emission and mass spectrometry measurements. Using the metrics of  $O_2(^1\Delta)$  yield and molar flow rate per unit reaction volume, the  $\mu$ SOG performs better than its macro scale counterparts. Future increases are possible, dependent on flow regime and chlorine utilization. The results obtained are very promising for COIL applications.

## ACKNOWLEDGEMENTS

The authors acknowledge J. Letendre for his expertise in building the experimental apparatus and D. Park for help with images of the SOG and optics. Additionally, the microfabrication expertise of Dr. Hanqing Li was critical to the success of the project. The Missile Defense Agency (MDA) and the Tactical Technology Office at DARPA generously provided funding for this research. The views and conclusions contained in this document are those of the authors and should not be interpreted as representing the official policies, either expressed or implied, of the Defense Advanced Research Projects Agency or the U.S. Government.

## REFERENCES

- [1] W. E. McDermott et al., "An electronic transition chemical laser," *Appl. Phys. Lett.*, vol. 32(8), 1975.
- [2] H. H. Wasserman and R. W. Murray, *Singlet Oxygen*. New York, New York: Academic Press Inc., 1979, p. 25.
- [3] S. Yoshida, H. Saito, and T. Fujioka, "New singlet oxygen generator for chemical oxygen-iodine lasers," *Appl. Phys. Lett.*, 49 (18), 1986.
- [4] K. R. Kendrick et al., "Determination of Singlet-Oxygen Generator Efficiency on a 10-kW Class Supersonic Chemical Oxygen-Iodine Laser (RADICL)" *IEEE J. Quantum Electronics*, vol. 35(12), pp. 1759-1764, 1999.
- [5] M. W. Losey et al., "Microfabricated Multiphase Packed-Bed Reactors: Characterization of Mass Transfer and Reactions," *Ind. Eng. Chem. Res.* 2001, vol. 40, pp. 2555-2562.
- [6] B. A. Wilhite et al., "Design of a MEMS-Based microChemical Oxygen-Iodine Laser ( $\mu$ COIL) System," *IEEE J. Quantum Electronics*, vol. 40 (8), pp. 1041-1055, 2004.
- [7] A. Günther, et al., "Micromixing of Miscible Liquids in Segmented Gas-Liquid Flow," *Langmuir*, vol. 21, pp.1547-1555, 2005.
- [8] K. A. Truesdell, S. E. Lamberson, G. D. Hager, "Phillips Laboratory COIL Technology Overview," AIAA 92-3003.
- [9] J. F. Hon et al., "A Heuristic Method for Evaluating COIL Performance," AIAA 94-2422.
- [10] W. T. Rawlins et al., "Spectroscopic Studies of a Prototype Electrically Pumped COIL System," SPIE Photonics West (2004), San Jose, CA.
- [11] W. Zhao et al., "Measures of the yield and chlorine utilization of singlet oxygen generator by uses of Raman spectroscopy," *Applied Optics*, vol. 42 (18), 2003.
- [12] M. V. Zaguidullin et al., "The sub- and supersonic COILs driven by jet type singlet oxygen generator," *SPIE*, vol. 3574, pp. 246-252.